

Coating versus Doping: Understanding the Enhanced Performance of High-Voltage Batteries by the Coating of Spinel $\text{LiNi}_{0.5}\text{Mn}_{1.5}\text{O}_4$ with $\text{Li}_{0.35}\text{La}_{0.55}\text{TiO}_3$

Valeriu Mereacre,* Pirmin Stüble, Vanessa Trouillet, Shamail Ahmed, Kerstin Volz, and Joachim R. Binder

$\text{Li}_{0.35}\text{La}_{0.55}\text{TiO}_3$ (LLTO) coated spinel $\text{LiNi}_{0.5}\text{Mn}_{1.5}\text{O}_4$ (LNMO) as cathode material is fabricated by a new method using hydrogen-peroxide as activating agent. The structure of the obtained active materials is investigated using scanning electron microscopy (SEM), transmission electron microscopy (TEM), X-ray diffraction (XRD), and X-ray photoelectron spectroscopy (XPS), and the electrochemical properties of the prepared cathodes are probed by the charge–discharge studies. The morphology of the coating material on the surface and the degree of coverage of the coated particles is investigated by the SEM, which shows a fully dense and homogeneous coating (thickness ≈ 7 nm, determined by TEM) on the surface of active material. XRD studies of the coated active materials treated at different temperatures (between 300 °C and 1000 °C) reveal expansion or contraction of the unit cell in dependence of the coating concentration and degree of Ti diffusion. It is concluded, that for the LNMO particles calcined at low temperatures, the LLTO coating layer is still intact and protects the active material from the interaction with the electrolyte. However, for the coated particles treated at high temperatures, Ti ions migrate into the structure of LNMO during the modification process between 500 °C and 800 °C, resulting in “naked” and unprotected particles.

problems, because the employed electrolytes contain organic flammable solvents. Therefore, the researchers are concentrating on lithium intercalation materials, which are more stable, easy to synthesize and can operate in the high voltage regime. One of the most promising candidate as high voltage cathode material is $\text{LiNi}_{0.5}\text{Mn}_{1.5}\text{O}_4$ (LNMO) spinel.^[1–4] It works in the voltage range of 3.5–5 V, has a practical capacity (about 130 mAh g⁻¹), low cost and provides a specific energy (≈ 600 Wh kg⁻¹), which is higher than that of many commercialized compounds. In addition, it has a very good electronic and ionic conductivity, and includes inexpensive manganese. However, this material has a weakness, which is widely discussed in the literature: an unstable interfacial stability between cathode and electrolyte, which slows down the broad practical use of such cathodes.^[5,6] The presence of Mn^{3+} in the structure of the LNMO is considered to be one of the causes for the short cycling and storage life

of a cell. Because of the disproportionation reaction of Mn^{3+} , the obtained Mn^{2+} ions may dissolve into the electrolyte and accelerate the capacity fade of the cell. The improvement of the electrochemical performance of such or similar cathode materials could be realized through suppression of the metal ions dissolution^[7] with help of a coating layer,^[8–11] which will protect the active material from direct contact with the electrolyte.

1. Introduction

The heavyweight designs and short lifespan of the Ni/MH, Ni/Cd, and lead acid batteries have forced the development of competing battery technologies based on rechargeable lithium-ion batteries. The main drawbacks of such batteries are, however, safety and overcharge protection, which are their intrinsic

V. Mereacre, P. Stüble, V. Trouillet, J. R. Binder
Institute for Applied Materials
Energy Storage Systems
Karlsruhe Institute of Technology
Hermann-von-Helmholtz-Platz 1, D-76344 Eggenstein-Leopoldshafen,
Germany
E-mail: valeriu.mereacre@kit.edu

P. Stüble
Helmholtz Institute Ulm
D-89081 Ulm, Germany
V. Trouillet
Karlsruhe Nano Micro Facility (KNMF)
Karlsruhe Institute of Technology
Hermann-von-Helmholtz-Platz 1, D-76344 Eggenstein-Leopoldshafen,
Germany
S. Ahmed, K. Volz
Department of Physics
Materials Science Center
Philipps-Universität Marburg
Hans Meerwein Str. 6, D-35032 Marburg, Germany

 The ORCID identification number(s) for the author(s) of this article can be found under <https://doi.org/10.1002/admi.202201324>.

© 2022 The Authors. Advanced Materials Interfaces published by Wiley-VCH GmbH. This is an open access article under the terms of the Creative Commons Attribution License, which permits use, distribution and reproduction in any medium, provided the original work is properly cited.

DOI: 10.1002/admi.202201324

LLTO ($\text{Li}_{0.35}\text{La}_{0.55}\text{TiO}_3$) has a good structural stability and a high lithium ion conductivity (up to 1 mS cm^{-1}) at room temperature.^[12] For that reason, in this study, it was selected as a coating material. In addition, LLTO displays these two properties not only in the crystalline form, but also in amorphous one, the last one offering more vacancies for lithium ion diffusion and transfer.^[13–15] This is a very important property, because at high temperatures, at which the LLTO crystallizes, a reaction between LLTO and active material might take place.^[16] Another positive aspect of a spinel coated with LLTO is that, unlike the inert coating layers (e.g., Al_2O_3), LLTO coating provides a conductive layer between spinel and the electrolyte, in this way facilitating the lithium-ion diffusion through the interface layer. As result, for the LLTO-coated LNMO spinel, a better electrochemical performance is expected.

The coating of different battery materials with LLTO-containing compounds is already well documented in the available literature.^[17,18] The most commonly used methods comprise solid state^[17] and sol-gel reactions.^[18] However, the use of these methods cannot guarantee a homogeneous and stable coating. In the case of solid-state reactions, the coating morphology and consistency are often difficult to control. Generally, the sol-gel method used to obtain coated materials has some specific advantages. But, although, the coating material obtained from such reaction is produced from a chemically homogeneous mixture, the final coated product frequently has regions that are better and others that are less protected against reactions with electrolyte.

The ALD (atomic layer deposition) method is believed to be the most suitable to produce ultra-thin coatings.^[19,20] But this technique requires very complex machines and is expensive to scale up. In this study, a novel, fast and low-cost synthetic approach was elaborated for the preparation of LNMO cathode materials with surface covered by a homogeneous and thin protecting layer of LLTO. To systematically study the deposition mechanism of a solid electrolyte as a coating material to cathode, scanning electron microscopy (SEM), transmission electron microscopy (TEM), X-ray photoelectron spectroscopy (XPS) and X-ray diffraction (XRD), combined with electrochemical property measurements were applied on both the original LNMO sample and the LLTO-coated ones. Furthermore, in order to distinguish between the contributions from the coating process itself and the influence of LLTO layer, the electrochemical measurements were done not only for the uncoated samples, but also for the uncoated samples treated at the same conditions as the coated ones.

2. Results and Discussion

2.1. Coating Material

The sol-gel method is very often used for preparation of different oxide powder products.^[21–24] Using this method, it is possible to obtain a gel with the highest homogeneity and one can have the highest control in converting the gel to oxide. As result, the sol-gel method seems to be most appropriate owing to the mixing of elements at molecular level during the synthesis. This method is also very often used for coating of battery materials.^[17,18]

In this work, the isolated LLTO powder was obtained using a sol-gel process and the same temperature handling as that for coated LNMO: under stirring the solution containing Li, La, and Ti ions was heated at about 100°C until a gel and later a dry powder was obtained. Crystalline LLTO powder was obtained by the calcination at 500 , 800 , and 1000°C in air and labeled as LLTO-500, LLTO-800, and LLTO-1000. SEM diagram of LLTO-1000 and X-ray diffraction patterns of the LLTO particles prepared by the calcination at three temperatures are shown in Figures S1 and S2 (Supporting Information), respectively.

The X-ray studies of the coating material at different temperatures (Figure S2, Supporting Information) resulted in powder diffraction patterns indicating that only at 800 and 1000°C the material are a crystalline LLTO oxide. The X-ray pattern at 500°C confirms the formation of an amorphous substance with an unknown structure. Relatively sharp reflections at 1000°C are observed and can be indexed to LLTO phase ($\approx 95\%$) and Li_2TiO_3 ($\approx 5\%$), while at 800°C broad reflections, which correspond to at least five components, are detected. The majority of the reflections at 800°C could be attributed to LLTO phase, while other could correspond to a mixture of TiO_2 , $\text{Li}_4\text{Ti}_5\text{O}_{12}$, Li_2TiO_4 , and/or $\text{Li}_{1.3}\text{Ti}_{1.7}\text{O}_4$ phases. Hence, the most probable component providing the coating layer on the surface of LNMO particles is anticipated to be LLTO. This is also confirmed by the elemental analysis and XPS studies of the coating and coated materials, calcined both at 800°C . Especially supportive is the elemental analysis for the LNMO-LLTO-800: the ratio between La and Ti was determined to be 1.60, which is very close to the ratio 1.62 calculated for $\text{Li}_{0.35}\text{La}_{0.55}\text{TiO}_3$.

In contrast to LLTO, the $\text{LiNi}_{0.5}\text{Mn}_{1.5}\text{O}_4$ coated with $\text{Li}_{0.35}\text{La}_{0.55}\text{TiO}_3$ oxide was synthesized by a new method using hydrogen peroxide as activating agent.

For the starting material LNMO, a specific surface of $0.35 \text{ m}^2 \text{ g}^{-1}$ was found. Based on the added educts to form 0.5 and 3 wt% of $\text{Li}_{0.35}\text{La}_{0.55}\text{TiO}_3$, a theoretical coating layer thickness of 2.9 and 17.1 nm is expected (calculated for crystalline LLTO, $\rho = 5 \text{ g cm}^{-3}$).

2.2. Scanning Electron Microscopy (SEM)

SEM images of the pristine, thermally treated, and coated $\text{LiMn}_{1.5}\text{Ni}_{0.5}\text{O}_4$ at different temperatures are shown in Figure 1. The particles show very regular truncated octahedral microstructure with large portions of (100) facets. To check if the heating process influenced the surface of LNMO, the uncoated sample was calcined at 800°C . The SEM image (Figure 1b) shows similar surface morphology and minor changes. The surface of the pristine and thermally treated at 800°C $\text{LiMn}_{1.5}\text{Ni}_{0.5}\text{O}_4$ particles is smooth and clean (Figure 1a,b), which indicates that the subsequent heating process has not essentially changed the micro-morphologies of the LNMO particles. On the contrary, the surface of the coated $\text{LiMn}_{1.5}\text{Ni}_{0.5}\text{O}_4$ become rougher and at 100 , 300 , 400 , and 500°C (Figure 1c–f, respectively) the LLTO coating layer is complete and homogeneous. At 600°C and higher, in addition to a uniformly distributed amorphous layer, clear crystalline nanoparticles of different morphology are observed (Figure 1g–i). In order to better identify the morphology of the obtained crystalline particles on the surface,

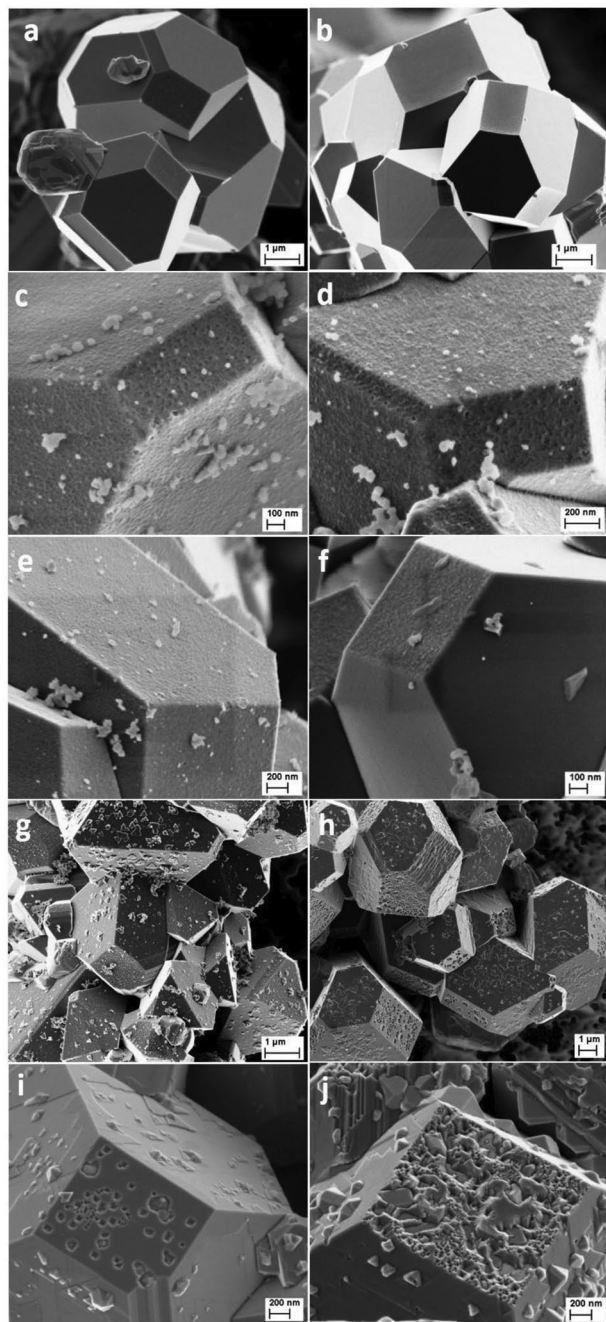


Figure 1. SEM diagrams of a) bare LNMO, b) bare LNMO calcined at 800 °C (used as reference), c) LNMO-LLTO-100, d) LNMO-LLTO-300, e) LNMO-LLTO-400, f) LNMO-LLTO-500, g) LNMO-LLTO-600, h) LNMO-LLTO-700, and i) LNMO-LLTO-800 and j) LNMO-LLTO-800 (with 3% LLTO). Samples from c) to i) are coated with 0.5% LLTO.

LNMO particles with increased LLTO coating amount ($\approx 3\%$) were prepared at 800 °C. SEM images of the obtained particles are shown in Figure 1j. The particles are covered by the uniformly distributed and overlapping crystalline nanosheets with impregnated tetragonal pyramids of different degree of crystallinity, both forms being considered to be LLTO. The subsequent calcination of this sample (LNMO-LLTO-800 (with

3% LLTO)) at 1000 °C resulted in particles (LNMO-LLTO-1000 (with 3% LLTO)) with very smooth surface (Figure 2). It looks like as LLTO particles have “melted” into surface of LNMO and formed a homogeneous and “polished” layer.

By comparing these eleven SEM images of particles with different surface morphologies (Figures 1 and 2) and their temperature evolution, it can be positively admitted that a coating material covers the surface of the prepared $\text{LiMn}_{1.5}\text{Ni}_{0.5}\text{O}_4$. The X-ray studies of the 3%-LLTO coated samples calcined at 800 and 1000 °C and XPS studies of 0.5%-LLTO coated samples and calcined at 700 °C and lower temperatures also confirm the presence of LLTO on the surface of LNMO particles. A more detailed visual analysis of the particle surface of the LNMO-LLTO-600, LNMO-LLTO-700, and LNMO-LLTO-800 samples, however, raises up some questions related to the integrity of the covering shell. An attempt to answer these questions will be made using X-ray powder diffraction and XPS studies (vide infra).

It also seems that no matter which concentration is taken for the coating, there are always some particles that are not coated on the surface of the active material (Figure 1c–f; Figure S3, Supporting Information). The reason could be that during the coating process a certain amount of the components of the coating material does not reach the surface of the LNMO particles before they react with each other and form other components like Li_2TiO_3 , $\text{Li}_x\text{Ti}_y\text{La}_z\text{O}_n$, etc. One of the reasons could be too high concentration of the coating material. Hence, a similar coating reaction was carried out, but only with 0.1% LLTO. The effect was the same: again, some particles of unknown composition are observed on the surface of the LNMO, even at 800 °C (Figure S3, Supporting Information). Conclusion: for this type of coating reaction, a certain amount of unidentified compositions is always expected under present reaction conditions.

It is also important to note that the coating reaction used in this work is relatively violent. To determine whether the surface structure of the bare LNMO was affected or not, a similar experiment was carried out, but without coating components. The SEM studies show particles with partially damaged surfaces, similar with the reported ones.^[25] In contrast, the surface of the coated particles is intact (Figure 1 and Figure S3, Supporting Information). It seems that the reaction between H_2O_2 and LNMO creates perfect conditions for the LLTO moiety to precipitate on the LNMO surface and instantaneously is protecting it from further reaction with the components of the reaction mixture.

2.3. Powder X-Ray Diffraction

Diffraction patterns of pristine LNMO and samples of uncoated LNMO and LNMO coated with 0.5 wt% and 3.0 wt% LLTO calcined at 300 °C, 500 °C, 600 °C, 800 °C, and 1000 °C were measured and refined. Selected patterns are shown in Figure 3, a collection of all patterns and refinements can be found in Figures S4–S6 (Supporting Information). All X-ray diffraction patterns reveal the presence of the main $\text{LiNi}_{0.5}\text{Mn}_{1.5}\text{O}_4$ -phase (MgAl_2O_4 structure-type, space group $Fd\bar{3}m$, $a \approx 817.3\text{--}818.3$ pm) and the presence of a rock-salt secondary phase, which was

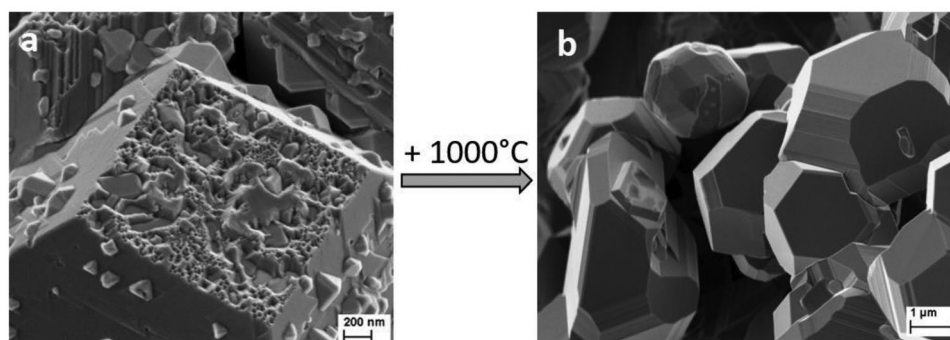
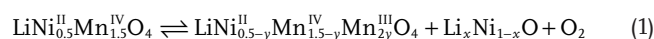


Figure 2. a) SEM diagrams of LNMO-LLTO-800 (with 3% LLTO) and b) of the same sample calcined additionally at 1000 °C.

refined as $\text{Li}_x\text{Ni}_{1-x}\text{O}^{[26]}$ ($x \approx 0.28$, NaCl-type, $Fm\bar{3}m$, $a \approx 414$ pm). Additional reflections, that could be assigned to crystalline coating material LLXO ($X = \text{Ti}, \text{Mn}$), are only observed for coated samples calcined at 800 °C and 1000 °C and were refined applying a structure model of $\text{Li}_{0.5}\text{La}_{0.5}\text{TiO}_3^{[27]}$ (trigonal perovskite structure, space group $R\bar{3}mH$, $a \approx 551$ pm, $c \approx 1335$ pm). Key results of the refinements are depicted in **Figure 4** and are listed in Table S1 (Supporting Information).

The pristine LNMO material was calcined at 900 °C and cooled to room temperature with 240 °C h^{-1} , resulting in 5.4(6) wt% $\text{Li}_x\text{Ni}_{1-x}\text{O}$ secondary phase and a LNMO phase with a rather high proportion of Mn(III). The latter becomes obvious from the increased LNMO lattice parameter of 818.04(2) pm, due to the higher ionic radius of Mn^{III} compared to Mn^{IV} (64.5 pm vs 53 pm).^[32] For a pure $\text{LiNi}^{\text{II}}_{0.5}\text{Mn}^{\text{IV}}_{1.5}\text{O}_4$ phase, which

is only accessible when calcining below the LNMO decomposition temperature (690 °C to 695 °C according to ref. [33]), a lattice parameter of, e.g., 816.4 pm^[34] to 817.0 pm^[35] are expected. As already discussed in detail for very similar materials back in 1993 by Feltz et al.,^[36] advocated by Cabana in the recent LNMO debate,^[34,37,38] and concluded from our preceding work,^[39] the higher Mn(III) content most likely is a side effect of the formation of the Ni-rich secondary phase, coming along with a Ni-depletion of the LNMO phase:



According to Equation (1), chemical equilibrium shifts to the right side when calcination is carried out above the decomposition temperature (often referred to as the oxygen release

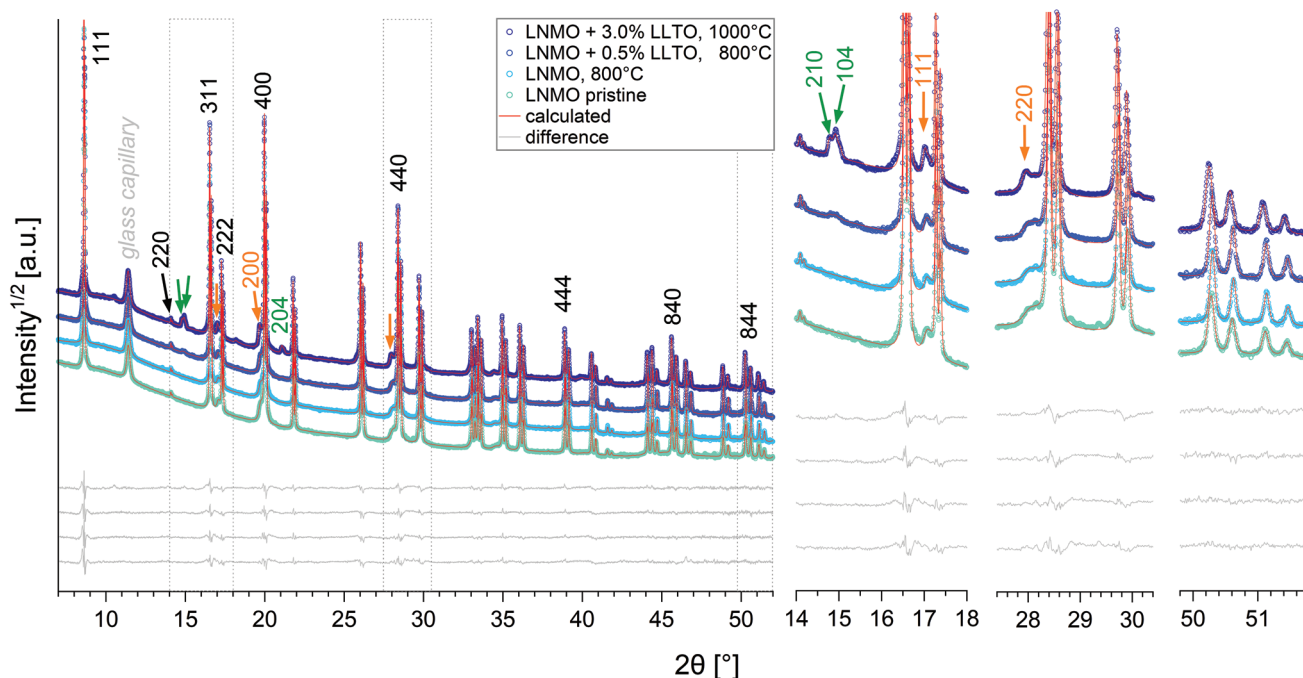


Figure 3. Selection of PXRD patterns with the corresponding Rietveld refinements: Pristine LNMO, LNMO treated at 800 °C, LNMO coated with 0.5% LLTO calcined at 800 °C and $\text{LiMn}_{1.5}\text{Ni}_{0.5}\text{O}_4$ with 3% LLTO and calcined at 1000 °C. The sections of 14° to 18°, 28.4° to 30.4° and 49.8° to 51.8° are enlarged to show crucial 2θ regions of the patterns. LNMO reflections are labeled black. The rocksalt secondary phase present in all samples is indicated in orange. Additional reflections attributed to a rhombohedral LLXO ($X = \text{Mn}, \text{Ti}$) phase are only found in samples calcined at 800 and 1000 °C and are labeled in green.

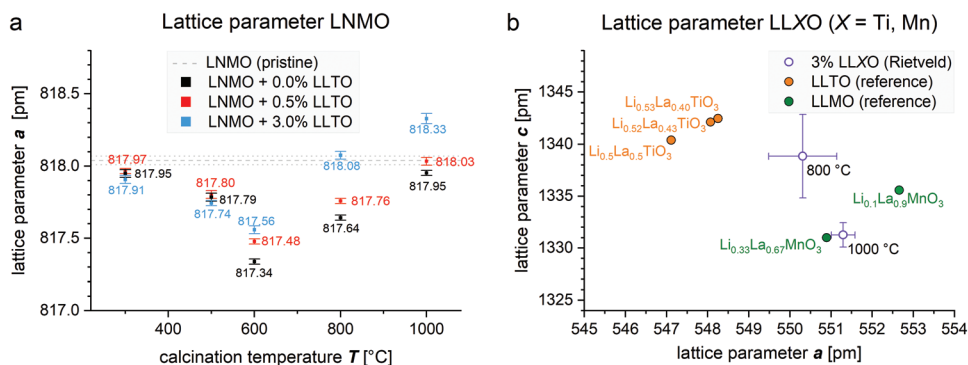


Figure 4. a) LNMO lattice parameters obtained for the starting material (gray, dots indicate the error range) and uncoated (black) and coated LNMO (red and blue) for the calcining temperatures 300 °C, 500 °C, 600 °C, 800 °C and 1000 °C. b) Lattice parameters of the LiLaXO_3 ($X = \text{Ti, Mn}$) side phase refined for the LNMO + 3% LLTO samples, calcined at 800 °C and 1000 °C (purple stars) compared to those of rhombohedral LiLaTiO ^[27–29] (orange) and LiLaMnO phases^[30,31] (green). Lattice parameters correspond to the hexagonal unit cell, space group $R\bar{3}cH$.

temperature) and to the left for lower calcination temperatures. However, the back reaction may be limited by excessive phase segregation and kinetic restraint.^[36] Accordingly, the lattice parameters of the samples calcined at 300 °C barely deviate from the pristine material, since there is hardly any oxygen uptake at this temperature. Upon calcining on 500 °C, larger proportions of the $\text{Li}_x\text{Ni}_{1-x}\text{O}$ phase transform back to the spinel phase and Mn(III) is partly oxidized to Mn(IV), which can be observed by the decreased LNMO lattice parameter. Together with a slightly increased cation mobility, found at 530 °C and above,^[33] the rock salt to LNMO transition is accelerated, leading to the minimum of the lattice parameters for the samples calcined at 600 °C ($a = 817.34(2)$ pm). An overall minimum of the lattice parameters would be expected for calcining temperatures around 700 °C, favoring the transformation of the disordered LNMO (space group $Fd\bar{3}m$) to the ordered phase ($P4_332$). However, since this work focuses on overwhelmingly disordered LNMO phases, calcining temperatures around 700 °C were spared herein. At 800 °C, which is a common calcining temperature for LNMO battery materials, a decent amount of Mn(III) and remains is present in the LNMO structure and the lattice parameter is increased compared to the 600 °C samples. Calcining the uncoated LNMO at 1000 °C finally yields a lattice parameter of 817.95(2) pm which again is very close to the 818.04(2) pm of pristine material calcined at 900 °C.

While the lattice parameters could be determined with high accuracy and reliability,^[23] the quantification of the rock-salt secondary phase ($\text{Li}_{1-x}\text{Ni}_x\text{O}$, space group $Fm\bar{3}m$, $a \approx 414$ pm) is rather error prone. Refinements yielded phase fractions of 4.5(4) wt% to 6.8(8) wt%, the individual values are listed in Table S1 (Supporting Information). As expected according to Equation (1), the values for 600 °C and 800 °C tend to be somewhat smaller compared to the starting material and the materials calcined at 300 °C and 1000 °C. However, due to the overlap of the reflections of the secondary phase with those of LNMO and the uncertainty regarding the Li/Ni ratio in $\text{Li}_x\text{Ni}_{1-x}\text{O}$, there is a high degree of uncertainty regarding the actual phase fraction. This is problem further amplified by the circumstance that newly formed domains of $\text{Li}_x\text{Ni}_{1-x}\text{O}$ are likely to be amorphous or nanocrystalline and thus are not visible in the XRD patterns.^[39]

However, powder X-ray diffraction is not only a suitable method to obtain information on the calcining temperature-dependent shift of the lattice parameter, but also can provide detailed information concerning for LNMO coating or doping effects: the lattice parameters of LNMO samples coated with 0.5 and 3% LLTO are likewise depicted in Figure 4a (red and blue marks). It becomes obvious, that for 300 °C and 500 °C the LNMO lattice parameters are literally the same for coated and uncoated samples, which indicates, that there is very little or no interaction of the bulk LNMO with the Ti and La-rich coating layer. This however, drastically changes at a calcining temperature of 600 °C and above. The LLTO coated LNMO samples show increased lattice parameters compared to uncoated LNMO, which thus must be related to the surface coating. It is well known from literature that manganese ions in LNMO can be substituted by Ti(IV)^[40–42] ions according to $\text{LiNi}_{0.5}\text{Mn}_{1.5-x}\text{Ti}_x\text{O}_4$ for ($0 < x < 1$),^[40] and that the Ti-related increase of lattice parameter can be described by Vegard's law. Based on the assumption, that for $T \geq 600$ °C all titanium present in the LLTO coating layer (composition $\text{Li}_{0.35}\text{La}_{0.55}\text{TiO}_3$) passes over into the LNMO phase, a lattice parameter increase of 0.07 pm and 0.42 pm is expected for 0.5% and 3% LLTO, respectively. As shown in Table 1, these calculated values are in very good agreement with the lattice parameter increases obtained by the Rietveld refinements for calcining temperatures of 1000 °C and 800 °C. The deviations of the experimental values from the calculated values for $T = 600$ °C might originate from kinetic

Table 1. Coating related lattice parameter increase. The observed values ($\Delta_{l.p.}^{\text{observed}}$) result from the Rietveld refinements, according to $\Delta_{l.p.}^{\text{observed}} = l.p.(\text{LNMO}^{\text{coated}}) - l.p.(\text{LNMO}^{\text{uncoated}})$. The calculated values ($\Delta_{l.p.}^{\text{calculated}}$) values correspond to the theoretical lattice parameter increase based on Vegard's law using the data of Kim et al.,^[40] assuming complete diffusion of Ti from the coating layer to the bulk LNMO.

Calcination temp.	LNMO + 0.5%LLTO		LNMO + 3%LLTO	
	$\Delta_{l.p.}^{\text{observed}}$	$\Delta_{l.p.}^{\text{calculated}}$	$\Delta_{l.p.}^{\text{observed}}$	$\Delta_{l.p.}^{\text{calculated}}$
600 °C	+ 0.14(4) pm	+ 0.07 pm	+ 0.22(5) pm	+ 0.42 pm
800 °C	+ 0.12(4) pm	+ 0.07 pm	+ 0.44(5) pm	+ 0.42 pm
1000 °C	+ 0.08(5) pm	+ 0.07 pm	+ 0.38(6) pm	+ 0.42 pm

limitations of the transition metal diffusion in LNMO, which is known to be limited at 600 °C.^[39,43]

Some studies on spinel-type LiMn_2O_4 (LMO) materials also suggest that partial substitution of manganese ions by lanthanum ions might likewise occur,^[44,45] which, however, is not supported by our results. First, La doping is hard to conceive due to the large differences in the ion radii (Ni^{II} : 69 pm, Mn^{III} : 64.5 pm, Mn^{IV} : 53 pm, Ti^{IV} : 60.5 pm vs La^{III} : 103.2 pm for coordination number 6)^[32] and secondly, the refinement of the diffraction patterns of the coated LNMO-LLTO materials calcined at 800 °C and 1000 °C reveal the presence of a suitable amount of LLXO ($X = \text{Ti}, \text{Mn}$) (cf. Figure 3 and Figure S5, Supporting Information and especially Figure S6, Supporting Information). As listed in Table S1 (Supporting Information), LLXO phase fractions of 0.5(2) wt% and 0.4(2) wt% for the samples LNMO+0.5% LLTO as well as 3.0(3) % and 3.6(3) % LLXO for LNMO+3.0% LLTO are obtained after calcining 800 °C and 1000 °C, respectively.

Since the reflections of this LLXO phase are rather weak, it is not possible to refine the phase composition based on the reflection intensities. However, refining the lattice parameters of the LLXO phase, which is possible for the LNMO+3%LLTO samples, yields decisive hints on its composition. As shown in Figure 4b, the lattice parameters deviate significantly from the values expected for LLTO phases like $\text{Li}_{0.5}\text{La}_{0.5}\text{TiO}_3$,^[28,29] but fit rather well to those observed for manganese phases LLMO, like, e.g., $\text{Li}_{0.33}\text{La}_{0.67}\text{MnO}_3$.^[30,31] Structurally, both are closely related crystallizing as trigonal perovskites in space group $R\bar{3}cH$ sharing the same basic Wyckoff sequence. The only difference is that in the manganese phase, Li and La share Wyckoff site $6a$, while in titanium phase, La exclusively occupies the $6a$ site, while Li is reported to occupy the $18d$ site. Even though mixed trigonal phases $\text{Li}_x\text{La}_y\text{Ti}_z\text{Mn}_{1-z}\text{O}_3$ to the best of our knowledge have not been reported yet, the existence seems quite plausible based on the similar ionic radii of manganese and titanium ions and the proven existence of isotypical edge phases $\text{Li}_x\text{La}_y\text{TiO}_3$ ($z = 1$) and $\text{Li}_x\text{La}_y\text{MnO}_3$ ($z = 0$).

On closer consideration, a composition deviating from LLTO is not even surprising, but is in fact mandatory, since it is obvious that titanium cannot diffuse into the LNMO phase and cause an increase in the lattice parameter, and at the same time form a quantitative amount of a LLTO phase on the surface.

Finally, the TEM (vide infra) images show that after calcining at high temperatures ≥ 800 °C, there is no longer a homogeneous coating layer on the LNMO surface, instead the LLXO phase is present in chunks of roughly 20 to 100 nm, leading to well-defined Bragg reflections in the diffraction patterns. The absence of corresponding reflections for the samples calcined at ≤ 600 °C can indicate both, a) that the doping layer maintains a predominantly amorphous or b) that it is crystalline, but does not yield detectable Bragg reflections due to the insufficient layer thickness (calculated: 3 nm and 17 nm for 0.5% and 3% LLTO).

To conclude, PXRD experiments are in full agreement with XPS and STEM results (vide infra) and lead to the conclusion that Ti doping of the LNMO phase is observed at $T \geq 600$ °C. In exchange, manganese ions from LNMO diffuse into the coating layer. At $T \geq 800$ °C and above, the amorphous coating layer transforms to a crystalline LLXO phase, where X is mainly Mn and some Ti. La doping of the LNMO phase is not observed, La ions remain at the surface of the LNMO particles.

2.4. XPS Measurements

To characterize the surface of the particles in dependence of the temperature, uncoated and coated samples were analyzed using XPS technique (Figure 5). Pristine LNMO shows clearly the characteristic Ni $2p_{3/2}$ and Ni $2p_{1/2}$ doublet as well as Mn 2p (not shown here) and Mn 3s. The splitting of this latter peak of $\Delta E = 4.5$ eV confirms the presence of Mn^{4+} .^[46] For the LLTO coated sample at 100 °C, a clear La 3d doublet can be observed as well as the corresponding Ti 2p doublet with Ti $2p_{3/2}$ at 458.6 eV. At the same time, almost no nickel can be detected since the observed peak at ≈ 855 eV belongs to the intense La

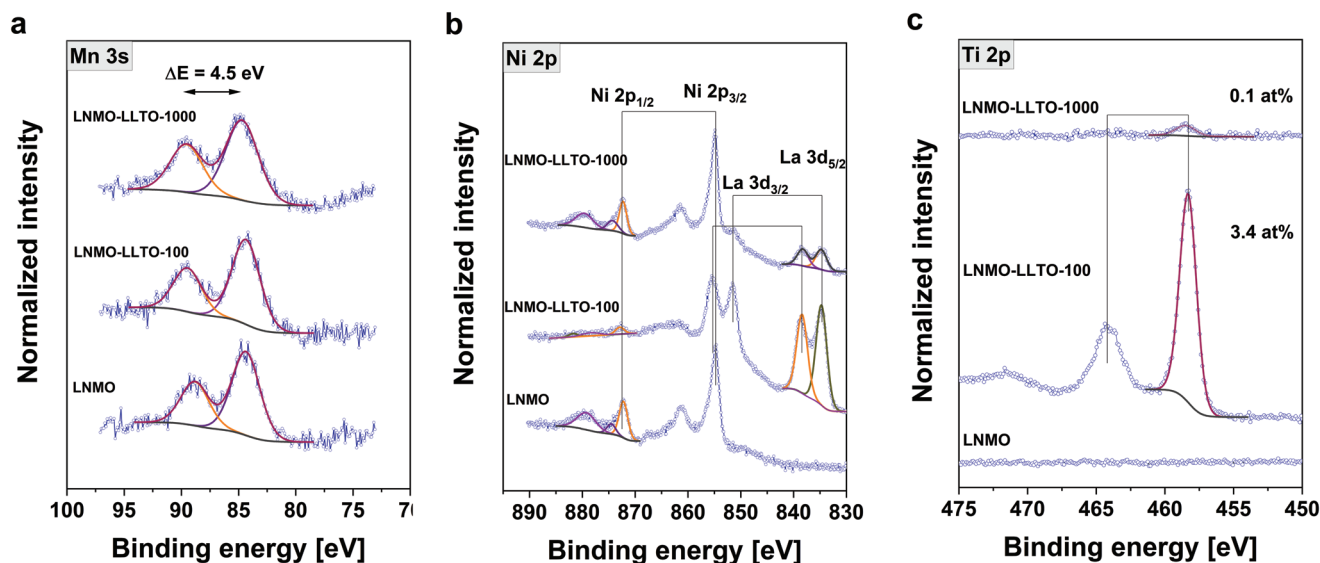


Figure 5. Mn 3s, Ni 2p, La 3d, and Ti 2p XPS spectra of uncoated (bottom) and coated samples at 100 °C (middle) and 1000 °C (top).

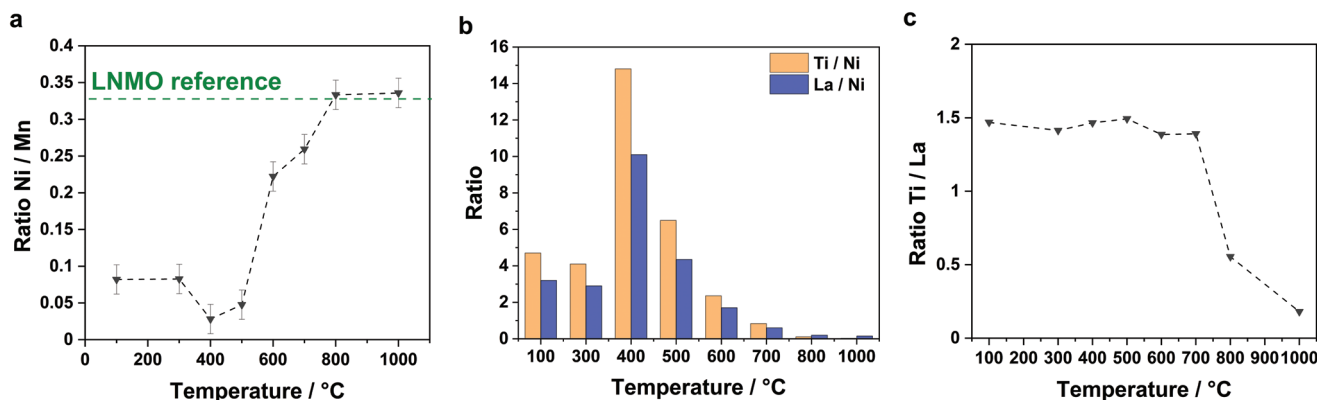


Figure 6. Ratio calculated from XPS quantitative analysis. a) Ni/Mn, b) Ti/ Ni and La/Ni, and c) Ti/La.

3d doublet. Ni $2p_{1/2}$ is well separated, shows a very weak intensity and is the peak taken in account to evaluate the concentration here (≈ 1 at%). The coated sample tempered at 1000 °C exhibits a very low content of Ti and some La. In order to follow the different concentrations on a similar way, Ti and La are considered in relation to Ni, the core signal, and for this purpose Ni $2p_{1/2}$ has to be taken in account since Ni $2p_{3/2}$ overlaps strongly with La $3d_{3/2}$.

Figure 6 depicts the evolution of the ratio Ni/Mn and Ti/La. The calculated ratio Ni/Mn based on the XPS quantitative analysis matches well with the theoretical one of 0.33 for uncoated LNMO (dashed green line). For 100, 300, 400, and 500 °C a homogeneous coating is observed from the SEM pictures (calculated layer thickness is ≈ 10 nm, STEM studies for particles treated at 500 °C provide a thickness of 7 nm) and confirmed by XPS with the presence of La and Ti. But not only LLTO is observed at the surface in this range of temperature. Mn is also clearly detected at the surface whereas Ni is present in a negligible amount like reflected by the low Ni/Mn ratio (Figure 6a).

Since the information depth of XPS is around 8 to 10 nm, the manganese belonging to the core particle is not supposed to be so easily detected and its concentration should correspond to Ni/Mn ≈ 0.33 . One of the reasons of the presence of Mn at the surface could be the partial dissolution of Mn ions during the coating reaction and their absorption into the LLTO coating layer. After 600 °C Ni/Mn is close to the expected value for LNMO which implies the presence of an only very thin LLTO layer at the surface or a not closed layer. Ti and La concentrations decrease reaching the zero position for Ti and a very weak amount for La. But this decrease does not follow exact the same curve for both elements. Until 700 °C the ratio Ti/La is very constant at a value of ≈ 1.5 supporting the presence of a stable LLTO layer at the surface whereas this ratio decreases strongly for 800 and 1000 °C (Figure 6b) implying a loss of Ti in the remaining very thin coating layer.

One of the reasons for such result could be the decomposition of the amorphous LLTO coating layer and almost complete diffusion of the Ti ions into the spinel structure. A very small quantity of the La ions detected by XPS method is explained by the formation of crystalline LiLaMnO particles distributed locally over the whole surface of LNMO particles. X-ray studies of the samples LNMO-LLTO-800 (with 3% LLTO) and (LNMO-LLTO-1000 (with 3% LLTO) also confirm the presence of

LiLaMnO (vide supra). The presence of minor quantities of Ti and Ni in the LiLaMnO particles is, however, not fully excluded.

In summary, using XRD and XPS studies it is concluded that the coating of the LNMO particles with LLTO was successful, but the obtained coating shell is integer only until 500 °C. At higher temperatures, the amorphous LLTO coating begins to crystallize, Ti ions are being diffused into LNMO and LNMO particles begin to “undress”, generating crystalline agglomerates of LiLaMnO.

2.5. STEM Measurements

The STEM-EDS analysis of LNMO-LLTO-500 sample is shown in **Figure 7**. The Ti and La elemental distribution maps indicate that the coating layer homogeneously covers the particle surface. Figure S7 (Supporting Information) EDS displays the spectrum from the coating region showing the Ti and La peaks.

Figure 8 displays the STEM-EDS analysis of LNMO-LLTO-800 sample. A uniform coating is not present on the surface of the particle. Also, the surface of the particle has a rough morphology with small facets, unlike the smooth surface present in the LNMO-LLTO-500 sample. La appears to have segregated in the form of small particles (which are most likely La_2O_3) on the surface, while Ti shows smeared distribution below the surface of the particle. Figure S8 (Supporting Information) shows EDS spectra from a La containing particle and from the region below the surface. The EDS spectra from the La-containing particle (marked as region “1” in Figure S8, Supporting Information) do not show a significant Ti peak. However, Ti could still be present in these positions in extremely low amounts that the current detection system may not have detected. The EDS spectrum from the sub-surface region (marked as region “2” in Figure S8, Supporting Information) shows a subtle Ti peak, highlighting that Ti might have diffused from the surface to the sub-surface regions due to high-temperature treatment.

2.6. Electrochemistry

For the electrochemical studies, several samples were selected: the pristine, the references (pristine heated at 500 °C and 800 °C, and coated samples heated at 500 °C and 800 °C. The

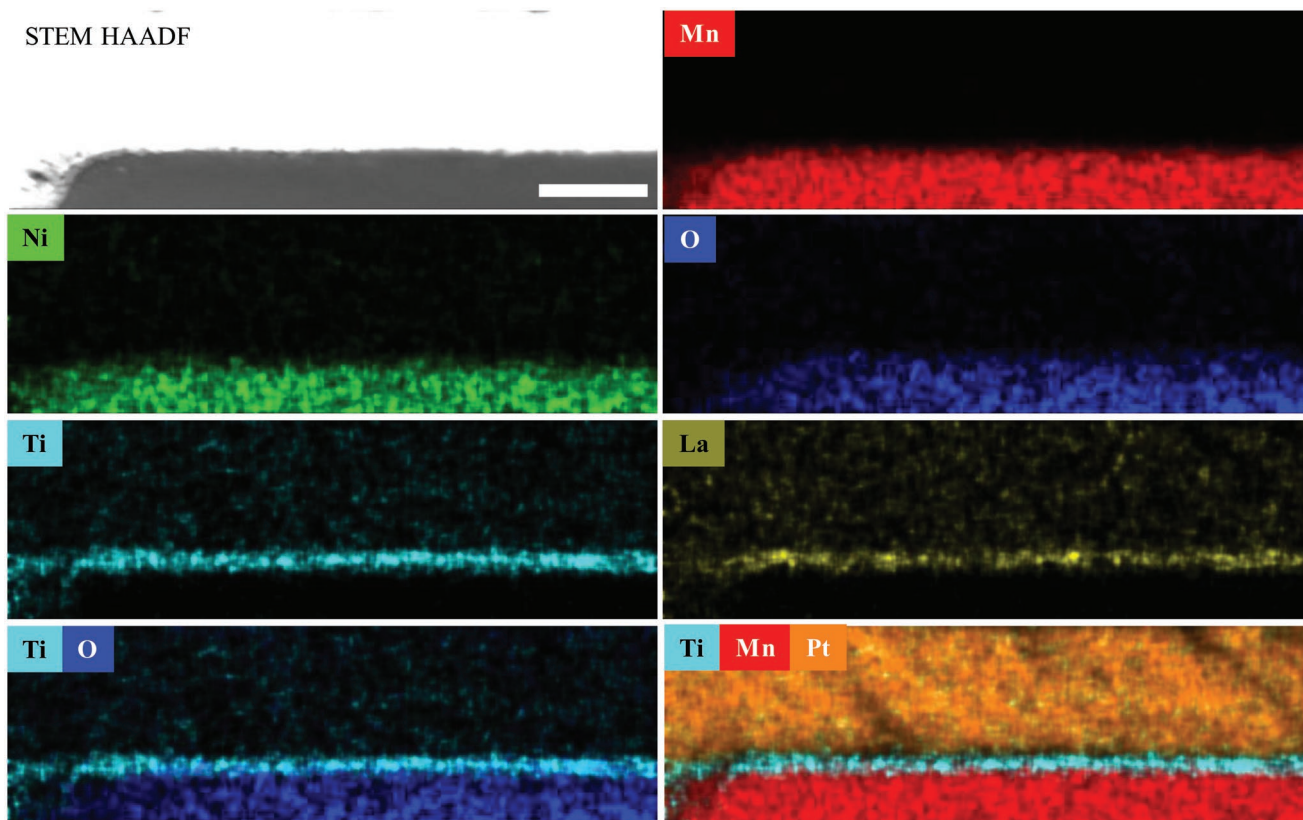


Figure 7. STEM-EDS analysis of LNMO-LLTO-500 sample. The top left figure is the STEM high-angle annular dark-field (HAADF) image. The rest of the figures are the corresponding EDS elemental distribution maps showing the distributions of Mn, Ni, O, Ti, La, and Pt. The scalebar is 50 nm in the HAADF image. The EDS spectrum of the coating region is shown in Figure S7 (Supporting Information).

electrochemical performance of uncoated and coated LNMO materials was assessed using coin-type half-cells at voltage window of 3.5–5 V. The differential capacity versus potential

(dQ/dV vs V) is shown in Figure S9 (Supporting Information). From the third cycle onwards, no significant alteration in the dQ/dV versus V behavior is observed. In the voltage region of

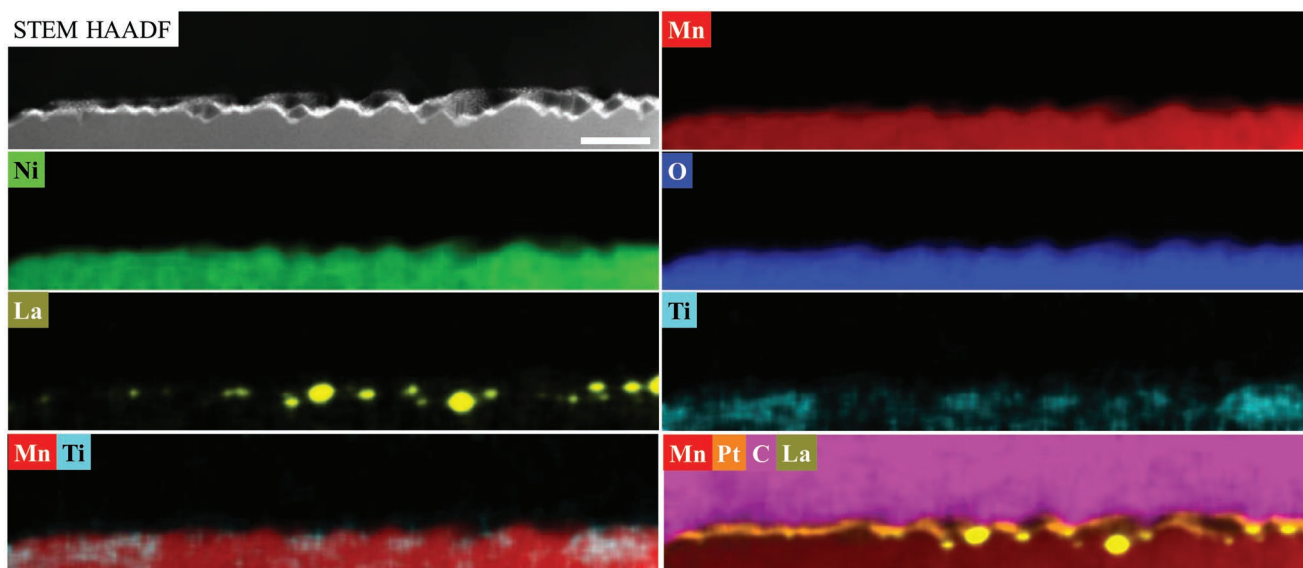


Figure 8. STEM-EDS analysis of LNMO-LLTO-800 sample. The top left figure is the STEM-HAADF image. The rest of the figures are the corresponding EDS elemental distribution maps showing the distributions of Mn, Ni, O, Ti, La, C, and Pt. The scale bar is 500 nm in the HAADF image. The EDS spectra of the selected regions are shown in Figure S8 (Supporting Information).

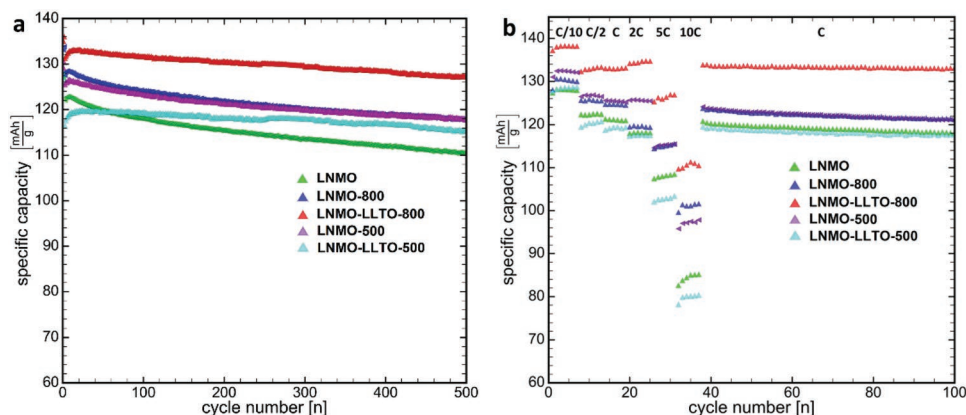


Figure 9. a) Capacity retention test at charge–discharge rate at C/2 – C (the first two cycles were done at 0.1 C) and b) rate capability test (the first cycle was done at 0.05 C; charge rate was C/2 without holding the voltage and discharge rates were varied as indicated in the figure) of five samples: bare (LNMO), bare calcined at 500 °C (LNMO-500), bare calcined at 800 °C (LNMO-800), coated and calcined at 500 °C (LNMO-LLTO-500) and coated and calcined at 800 °C (LNMO-LLTO-800).

4.7–4.8 V two pairs of redox peaks related to the Ni²⁺/Ni³⁺ and Ni³⁺/Ni⁴⁺ couples are observed. A broad and weak peak associated with the Mn³⁺/Mn⁴⁺ couple is also observed at about 4 V, indicating the presence of disordered *Fd-3m* phase.

The cycle-life performances of the pristine and references (calcined pristine at 500 and 800 °C) are given in Figure 9. Figure 9a compares the cycling performances of the bare LNMO, LNMO-500, and LNMO-800 electrodes at 1 C rate (the first two cycles were done at 0.1 C). The initial capacity of all electrodes shows insignificant differences in dependence of the temperatures: 127.7, 130.2, and 133.8 mAh g⁻¹, respectively. The small differences are supposed to be the result of positive influence of additional thermal treatment (500 or 800 °C) on the crystal structure.^[39] All electrodes show the same degree of capacity fading. In addition, the rate capability test (Figure 9b) also shows minor differences, especially between C/2 and 5 C.

It should be mentioned, that in general all uncoated active materials analyzed in this work show a relatively good long-term capacity fading and capacity retention. These properties seem to depend on the surface orientations of the octahedral spinel particles, which normally consist entirely of (111) surfaces. However, the particles examined in this work contain large portions of truncated (100) surfaces, which stabilize the spinel structure and can promote lithium ion transport.^[47]

The long-term cycling performance of bare LNMO and LNMO calcined at 500 °C (LNMO-500), 800 °C (LNMO-800), coated and calcined at 500 °C (LNMO-LLTO-500) and coated and calcined at 800 °C (LNMO-LLTO-800) are given in Figure 9a. The cells were initially charged–discharged two cycles at 0.1 C, and then charged (at 0.5 C) and discharged (at 1 C) 500 times with the voltage of 3.5–5.0 V. The bare LNMO, LNMO-500, and LNMO-800 at 1 C show initial capacities of ≈122.5, 125.9, and 128.0 mAh g⁻¹, respectively, however, all electrodes show a comparable degree of capacity fading: after 500 cycles the remained capacity for the original LNMO is 89.9%, for LNMO-500 is 93.7% and for the LNMO-800—91.8%. On the other hand, LNMO-LLTO-800 and LNMO-LLTO-500 show a much higher stability and capacity retention: for the LNMO-LLTO-500 the remained capacity is 96.2% and for LNMO-LLTO-800—95.4%. Strikingly, the last two cathode materials show a very

different initial capacity: ≈119.3 and ≈132.8 mAh g⁻¹, for LNMO-LLTO-500 and LNMO-LLTO-800, respectively. In fact, these two temperatures, 500 °C and 800 °C, were chosen deliberately to identify the influence of the crystallinity of the coating material on the electrochemical performance of the cathode materials. Taking into consideration the conclusions made in the XRD and XPS sections, it is assumed, that such a big difference of the initial capacity could be due to different structure of the coating layer: LNMO-LLTO-500 is coated, but the coating is amorphous and LNMO-LLTO-800 has almost no coating, but it is doped with Ti ions (Figure S2, Supporting Information see the X-ray of LLTO at 500 °C and 800 °C). The Ti-substitution results in a higher degree of disordering of the transition metals and subsequently will lower the symmetry of the spinel. As result, the obtained material has a faster lithium ion diffusion, is more stable at high operating voltages and has a higher capacity than Ti-free pristine material.^[40–42] The coating layer acts as a protection layer, preventing the active material from direct communication with electrolyte, in this way suppressing the dissolution of metal ions. From the electrochemical results of these two samples, one can conclude that there is no big difference between the protection effects of the coating layer obtained at different temperatures. The smaller capacity of LNMO-LLTO-500 material could be because of the reduced ionic conductivity of the amorphous coating material. This will also result in a somewhat higher resistance, which is reflected in the slightly higher polarization (see dQ/dV plot, Figure S9, Supporting Information). It is known that the atomic packing in amorphous LLTO is less dense than in the crystalline one.^[48] As a result, the amorphous LLTO has more and larger free volumes for Li ions to move. Nevertheless, the ionic conductivity is still low, ≈10⁻⁶ S cm⁻¹, in comparison to crystalline LLTO, which reach a lithium-ion conductivity up to 10⁻³ S cm⁻¹ at room temperature.^[12] It should be mentioned here that we are not aware about the actual structure of the amorphous coated material at 500 °C. Based on the PXRD for the crystalline coating material obtained at 800 °C there is a mixture of at least four phases. The amorphous LLTO obtained at 500 °C can contain the same or even different other phases. The electrochemical investigations, however, show that the coating obtained at 500 °C has a

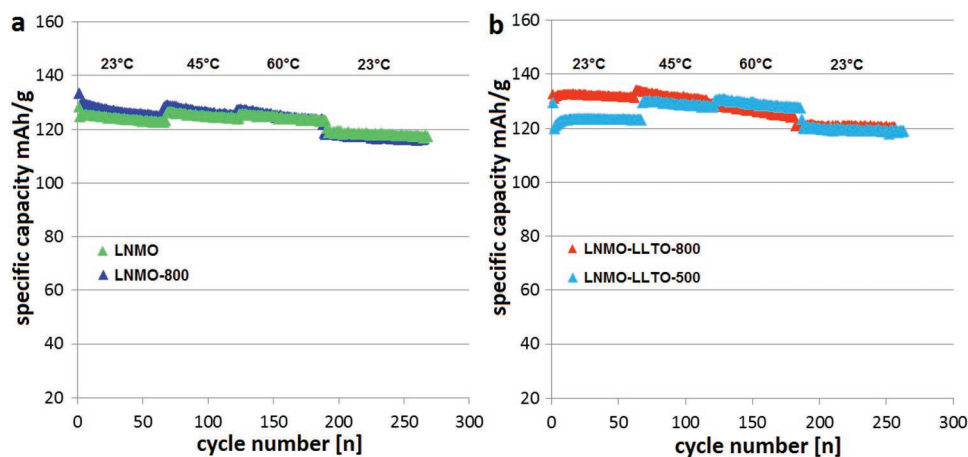


Figure 10. Capacity retention test at charge–discharge rate at 1 C (the first cycle was done at 0.1 C) for a) LNMO and LNMO-800 and b) LNMO-LLTO-800 and LNMO-LLTO-500 at different temperatures (23 °C, 45 °C, and 60 °C).

positive protective function, which leads to very good stability and capacity retention of 96.2% after 500 cycles.

To probe the structural stability in more detail, cycling performance was assessed at different temperatures of 23, 45, and 60 °C at 1 C as shown in **Figure 10**. Initially, every cell was charged–discharged one cycle at 0.1 C for the activation. During the first ≈65–75 cycles at 23 °C all four electrodes show similar capacity evolution as other cells (shown in Figure 9a). However, when the temperature was raised to 45 °C, a sudden increase in the capacity took place. Due to the increase of the ionic and electronic conductivity with temperature, theoretically, it is expected to observe such a trend of the capacity retention at higher temperatures. Unexpected is, however, a much higher “jump” (from 122.9 to 130.0 mAh g⁻¹) in the case of LNMO coated and treated at 500 °C in comparison to the electrode prepared from LNMO coated and treated at 800 °C (from 131.2 to 134.1 mAh g⁻¹). If the LNMO-LLTO-800 sample would have been coated, then, due to the higher ionic conductivity of the LLTO crystalline form in comparison with the amorphous LLTO, one would expect a better or at least the same improvement of the electrochemical performance for the crystalline form. This is not the case here. Another unexpected trend of the capacity retention for these two electrodes became even more significant at 60 °C: the LNMO-LLTO-500 shows a further increase in the capacity when the temperature is raised from 45 to 60 °C (Figure 10a). On the other hand, the LNMO-LLTO-800 displays an opposite development—a decrease in the capacity and a quicker degradation. Since side reactions with the electrolyte and, respectively, decomposition of the active material increase at elevated temperatures, the role of the crystalline coating material at 800 °C was expected to be protection of the cathode material. But in this case, it seems that the LNMO-LLTO-500, covered with an amorphous material, exhibits a more robust cycling performance in the extended cycles and high temperatures areas than LNMO-LLTO-800 protected by a crystalline LLTO. This fact, again, confirms the conclusions extracted from the XRD and XPS studies, that the coated sample calcined at 800 °C represents a “naked,” inhomogeneously coated and doped LNMO material, but the sample coated and calcined at 500 °C is a pure LNMO, homogeneously coated with amorphous LLTO. As result, due to the side reactions with

the electrolyte at elevated temperatures, the LNMO-LLTO-800 will degrade faster, than the sample LNMO-LLTO-500. As was earlier reported, inorganic materials can show good protecting properties for the surface of cathode materials, but they do not improve the electrochemical performance of the studied LNMO samples.^[49,50] Obviously, the amorphous coating layer of LLTO analyzed in this study has not only good protecting properties, but also shows a positive contribution to the stability and electrochemical performance of the studied electrodes at elevated temperatures. A still open question is, however, what is the real structure/composition of the coating material at 500 °C. This question will be answered in a different study.

The rate capability test is an important property of the battery under investigation because the charging/discharging time of batteries in electronic devices depends on the speed of the Li-ion extraction and insertion from and into the cathode material. The rate capability test of the pristine, thermally treated uncoated, and coated spinel were run in the same range of 3.5–5.0 V and at different rates from 0.1 to 10 C (Figure 9b). The cells were first charged–discharged at a current density of 0.05 C for one cycle, six cycles at 0.1 C and six cycles 0.5 C. Then they were charged with 0.5 C rate and discharged at 1, 2, 5, and 10 C rates, respectively. After 10 C, the cells were further cycled at 1 C. Once the discharge rate increases from 0.1 to 10 C, the discharge capacity of the bare LNMO decreases from 1274 to 84.8 mAh g⁻¹, which is 66.5% capacity retention. The LNMO-800 shows 77.1% (from 129.9 to 100.2 mAh g⁻¹), LNMO-500—73.7% (from 132.2 to 97.5 mAh g⁻¹), LNMO-LLTO-500—62.5% (from 127.4 to 79.7 mAh g⁻¹) and LNMO-LLTO-800 shows 79.6% (from 138.3 to 110.1 mAh g⁻¹) capacity retentions. Hence, the rate capability of the LNMO cathode was improved both by the additional heat treatment (as revealed by the capacity difference between LNMO and LNMO-500/LNMO-800) and coating process, with the higher capacity retention, better performance and much higher degree of stability obtained for the sample which was coated and heated at 800 °C. As in case of capacity retention test (vide supra), it is concluded that the improvement of the rate capability of this compound could also be attributed to effect of Ti substitution for Mn.^[40,41]

As revealed in Figure 9b, the discharge capacities of the initial several cycles for LNMO-LLTO-800 show a growing trend:

the capacity ($\approx 133.3 \text{ mAh g}^{-1}$) at 2 C is slightly higher than that at lower current densities (0.5 and 1 C). Such a phenomenon is not new and it is suggested that during the first cycles the electrodes are being wetted and activated, and as a result a larger capacity later is obtained.^[47,51,52] Remarkably, a capacity of about 133.6 mAh g^{-1} , higher than the initial capacity (132.8 mAh g^{-1} at 1 C), can be recuperated when the current density proceeds to 1 C once the electrode was cycled at high rates. This indicates that the “formation” time and activation processes of the electrodes with coated LNMO need a relatively longer time. The last effect was not observed for other four materials: LNMO, LNMO-500, LNMO-800 and LNMO-LLTO-500.

3. Conclusion

In summary, we revealed the major enhancement of the capacity retention and rate capabilities of a spinel LNMO cathode material by the applying a fast ionic conduction solid electrolyte coating. The possibility of synthesis of homogeneously LLTO-coated $\text{LiNi}_{0.5}\text{Mn}_{1.5}\text{O}_4$ material, using hydrogen peroxide as activating reagent, was demonstrated. It proved to be a very fast, efficient, and low-cost approach. The successful deposition of the LLTO coating was supported by the STEM, SEM, XRD, and XPS studies. The SEM results show the crystallization development of the coating material with increasing temperature and directly indicates the presence of the coating sample on the LNMO surface. Information about chemical environments of the Ti and La elements of the coated samples was obtained from the XPS studies.

The X-ray studies of pure coating material at different temperatures confirm the formation at 500 °C of an amorphous and at 800 °C, and higher temperatures, of a crystalline phase. From the capacity retention tests, a major enhancement of the electrochemical properties associated with the coating layer was observed. In addition to the very good cycling performance, the rate capability tests also reveal that the coated materials exhibit enhanced reversibility and stability. As a key factor affecting the electrochemistry of the coated active materials could be regarded the high ionic conductivity of LLTO. Compared with the LNMO coated with LLTO and calcined at 800 °C, the LNMO coated with amorphous LLTO (calcined at 500 °C) shows a slightly lower capacity, but a better cycling performance in the extended cycles and, especially, at elevated temperatures. Combined XRD, XPS, and STEM studies reveal that for the LNMO particles calcined at 500 °C, a LLTO coating layer is present at the surface and protects the active material from the interaction with the electrolyte. At 600 °C, cation exchange between the LLTO coating layer and the spinel phase leads to partial Ti doping of LNMO and an enrichment of manganese in the (still amorphous) surface layer LLXO (X = Mn, Ti) is observed. At 800 °C and above, most of the titanium from the coating layer diffuses into the LNMO phase. In exchange, the LLXO phase on the surface becomes rather Mn rich. At these temperatures, the uniform coating layer gets lost, instead isolated crystalline LLXO particles are found on the surface. The enhancement of the electrochemical properties of the LNMO treated at 800 °C is assumed to be not because of the coating layer, but because of LNMO doping with Ti ions. La doping of the spinel phase is not observed.

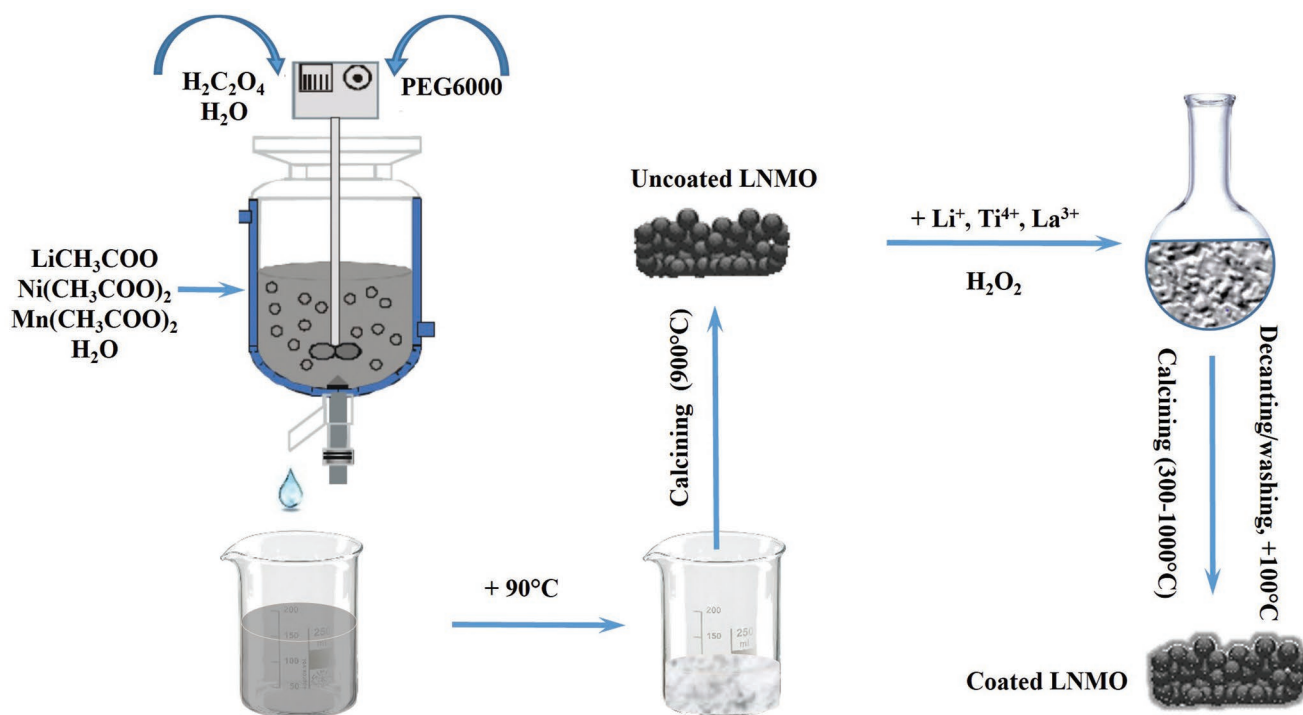
This study shows that the cathode materials can also be coated with amorphous coatings, which will not only improve the stability of the cathode active materials, but can be synthesized under “milder” conditions than the crystalline equivalents. A further study of LLTO coating could also be carried out on other cathode materials (e.g., layered oxides). Such work is under way and will be reported in the near future.

4. Experimental Section

Materials Preparation: The precursor for LNMO was obtained by a coprecipitation technique described elsewhere.^[25] In a typical synthesis route (**Scheme 1**), 0.185 mol of analytical reagent grade $\text{LiCH}_3\text{COO} \cdot 2\text{H}_2\text{O}$, 0.090 mol $\text{Ni}(\text{CH}_3\text{COO})_2 \cdot 4\text{H}_2\text{O}$, and 0.270 mol $\text{Mn}(\text{CH}_3\text{COO})_2 \cdot 4\text{H}_2\text{O}$ (all supplied by Alpha Aesar, Kandel, Germany) were dissolved in 300 mL of water. The obtained solution was transferred into a 1 L continuously stirred tank reactor.^[53] Separately, 0.451 mol of $\text{H}_2\text{C}_2\text{O}_4 \cdot 2\text{H}_2\text{O}$ were dissolved in 450 mL of water. Under temperature of 50 °C and constant stirring (400 rpm) of the Li-Ni-Mn solution, 30 g of solid PEG6000 was added. After 10 min, when PEG6000 dissolved completely, the oxalic acid aqueous solution was started to be pumped (10 mL min^{-1}) into the continuously stirred tank reactor. After the oxalic acid solution was completely pumped, the reaction mixture was stirred for additional 20 min. Then, the obtained suspension was dried at 90 °C to obtain a green viscous precursor ($\approx 85 \text{ g}$). The resultant precursor was calcined in air at 450 °C for 4 h and then at 900 °C for 24 h, and cooled down to room temperature with the heating and cooling rate of $4 \text{ }^\circ\text{C min}^{-1}$ to obtain the $\text{LiMn}_{1.5}\text{Ni}_{0.5}\text{O}_4$, which is labeled as LNMO. Brunauer-Emmett-Teller (BET) surface area is $0.35 \text{ m}^2 \text{ g}^{-1}$. The reference compounds, LNMO-300, LNMO-500, LNMO-600, LNMO-800, and LNMO-1000 were obtained by calcining pristine LNMO in air at 300, 500, 600, 800, and 1000 °C, respectively, using the following program: 250 °C for 2 h and then heated at the indicated temperature for 5 h, and cooled down to room temperature with the heating and cooling rate of $4 \text{ }^\circ\text{C min}^{-1}$.

Preparation of Li-La-Ti Coating Solution: Reagent-grade lithium acetate ($\text{LiOOCCH}_3 \cdot 2\text{H}_2\text{O}$), lanthanum nitrate ($\text{La}(\text{NO}_3)_3 \cdot 6\text{H}_2\text{O}$) and titanium isopropoxide ($\text{Ti}(\text{C}_2\text{H}_5\text{O})_4$) (all supplied by Aldrich, Steinheim, Germany) were used as lithium, lanthanum, and titanium sources. Two solutions were prepared: 0.136 g $\text{LiOOCCH}_3 \cdot 2\text{H}_2\text{O}$ and 0.793 g $\text{La}(\text{NO}_3)_3 \cdot 6\text{H}_2\text{O}$ were dissolved in 10 mL water free (absolute) ethanol. Separately, 0.966 g $\text{Ti}(\text{C}_2\text{H}_5\text{O})_4$ was dissolved in 30 mL H_2O_2 (30%). Under magnetic stirring of the first solution, the second one was added. The obtained mixture was stirred until a clear Li-La-Ti solution was obtained.

Material Coating: In a round bottom flask (300 mL) with 1.5 g LNMO, under stirring, 10 mL H_2O_2 (30%) was added. After $\approx 1 \text{ min}$, 0.5 mL Li-La-Ti coating solution was added. During the next 2 min, the reaction was relatively silent, but after this time, the reaction started to be very violent with forming of a white fog. The violent reaction takes place in less than 2 min. After additional 5 min of stirring, the reaction mixture was decanted and the obtained powder washed with 100 mL water (two times) and dried during 1 h at 100 °C. The obtained dry powder (LNMO-LLTO-100) was divided in seven portions and calcined in air at $T = 300, 400, 500, 600, 700, 800$ and 1000 °C using the following program: 250 °C for 2 h and then heated at particular temperature for 5 h, and cooled down to room temperature with the heating and cooling rate of $4 \text{ }^\circ\text{C min}^{-1}$. Scheme 1 illustrates a schematic diagram of the synthetic process. The quantity of the $\text{Li}_{0.35}\text{La}_{0.55}\text{TiO}_3$ expected to be coated on the surface of LNMO particles is around 0.5%. The obtained samples were labeled as LNMO-LLTO-300, LNMO-LLTO-400, LNMO-LLTO-500, LNMO-LLTO-600, LNMO-LLTO-700, LNMO-LLTO-800, and LNMO-LLTO-1000 respectively. A similar reaction was made with 3 mL Li-La-Ti coating solution, resulting in LNMO particles coated with approximately 3 wt% LLTO. The obtained sample was divided into two portions and calcined in air at $T = 800 \text{ }^\circ\text{C}$ and 1000 °C, and labeled as LNMO-LLTO-800(3%) and LNMO-LLTO-1000(3%), respectively.



Scheme 1. Schematic diagram of the synthetic and coating processes.

Coating Preparation: 10 mL of the Li–La–Ti coating solution was used to prepare pure LLTO in crystalline form. Under stirring, the solution was heated on a hot plate at about 100 °C until a dry powder was obtained. Amorphous or crystalline LLTO powder was obtained by the calcination of the obtained dried powder at 500 °C, 800 °C, and 1000 °C in air and labeled as LLTO-500, LLTO-800, and LLTO-1000. The calcination program was the same as for the coated LNMO-LLTO samples.

Powder X-Ray Diffraction and Scanning Electron Microscope: Powder X-ray diffraction (PXRD) for the pure LLTO samples (LLTO-500, LLTO-800, and LLTO-1000) (Figure S2, Supporting Information) was carried out using Stadi P diffractometer (Stoe, Germany) equipped with a Dectris Mythen 1K detector (Transmission geometry, Mo-K α 1—radiation).

Diffraction patterns of LNMO and LLTO-coated LNMO powders were investigated on an advanced in house PXRD setup optimized for tracing structural changes in energy materials. Herein, a multisample capillary spinner is mounted on a Huber six-circle diffractometer equipped with a molybdenum rotating anode (Mo-K α radiation) and a 2D Pilatus 300K-W detector. A detailed description of the setup can be found in the previous publication.^[23] The serial measurements were carried out with a sample to detector distance of 0.7 m. The diffraction patterns obtained were refined by the Rietveld method using the Topas6 Software (Bruker).

A scanning electron microscope SEM (Zeiss Supra 55, Oberkochen, Germany) was used to elucidate the morphology of precursor, coating material, and coated samples. Before measurement, the samples were prepared by the mounting the powder on adhesive carbon tape.

Specific Surface Determination: The specific surface area ($A_{\text{BET}} = 0.35 \text{ m}^2 \text{ g}^{-1}$) of the starting material was analyzed using nitrogen physical adsorption isotherms measured with a Gemini VII 2390 (Micromeritics GmbH).

Scanning Transmission Electron Microscopy: The samples for scanning transmission electron microscopy (STEM) energy-dispersive X-ray (EDS) analysis were prepared via JEOL JIB-4601 focused-ion beam/scanning electron microscope (FIB/SEM). A thin layer of Pt was first coated on the surface of the particles before loading to the FIB. Then C and W layers were deposited using a Ga-ion beam. The sample was initially thinned down with a 30 kV Ga-ion beam and finally polished with a 5 kV Ga-ion beam.

A double Cs-corrected JEOL JEM-2200FS transmission electron microscope operating at 200 kV was used for the STEM-EDS analysis.

The EDS data was acquired with Bruker XFlash 5010 detector. The EDS data analysis was done by using Bruker ESPRIT 2.3 software.

X-Ray Photoelectron Spectroscopy: XPS measurements were performed using a K-Alpha+ XPS spectrometer (ThermoFisher Scientific, East Grinstead, UK). Data acquisition and processing were conducted with the Thermo Avantage software. All powders were analyzed using a microfocussed, monochromated Al K α X-ray source (400 μm spot size). The K-Alpha+ charge compensation system was employed during analysis, using electrons of 8 eV energy, and low-energy argon ions to prevent any localized charge build-up. The spectra were fitted with one or more Voigt profiles (BE uncertainty: $\pm 0.2 \text{ eV}$) and Scofield sensitivity factors were applied for quantification.^[54] All spectra were referenced to the C 1s peak (C–C, C–H) at 285.0 eV binding energy controlled by means of the well-known photoelectron peaks of metallic Cu, Ag, and Au, respectively.

Electrochemical Measurements: Electrochemical measurements were carried out via galvanostatic charge/discharge cycling using 2032 coin cells with lithium metal as the anode on an BT2000 battery cycler (Arbin Instruments, College Station, TX, USA). During electrode preparation, the slurry was a mixture of 80 wt% active material, 10 wt% Super-S carbon black (Timcal, MTI Corporation, Richmond, CA, USA) and 10 wt% PVDF (polyvinylidene fluoride) with NMP (1-methyl-2-pyrrolidinone) as solvent. Electrodes were prepared by the coating the slurry on an Al foil with a 200 μm notch bar spreader and dried in air at 80 °C for 20 min, then at 100 °C for 16 h in vacuum. Usual cathode loadings were in the range of 4.0–5.0 mg cm^{-2} ; an electrode diameter of 12 mm was used. Before using the cathode disks were pressed in a hydraulic press to 6 kN and dried additionally for 60 min in a vacuum oven at 110 °C. The electrolyte was 1.0 M LiPF₆ solution in 1:1 v/v ethylene carbonate:diethyl carbonate (EC:DMC). As anode a lithium metal foil (diameter 12 mm) was used. As separators were used one layer of Celgard 2325 (Celgard, Sélestat, France) on the lithium and one layer on the positive electrode, and one GFC microfiber separator in the middle. Cells were assembled in a dry Ar-filled glove box. Cycling was performed at temperatures of 23, 45, and 60 °C. A voltage window of 3.5–5.0 V versus Li⁺/Li was applied.

Elemental Analysis: Elemental analysis (EA) was done at the IAM-AWP, Chemical analysis laboratory, KIT, using inductively coupled plasma optical emission spectrometry (ICP-OES, iCAP 7600 DUO, Thermo

Fisher Scientific GmbH, Dreieich, Germany) to determine the Li, La, Mn, Ni and Ti elements (Table S2, Supporting Information).

Supporting Information

Supporting Information is available from the Wiley Online Library or from the author.

Acknowledgements

This work was carried out with the support of the Helmholtz Energy Materials Foundry (HEMF), a large-scale distributed research infrastructure founded by the German Helmholtz Association. It also contributes to the research performed at CELEST (Center for Electrochemical Energy Storage Ulm-Karlsruhe). S.A. and K.V. gratefully acknowledge the funding from Bundesministerium für Bildung and Forschung (BMBF) within the FESTBATT cluster of competence (project 03XP0433C). The authors also thank Margarete Offermann for support on surface area analysis.

Conflict of Interest

The authors declare no conflict of interest.

Data Availability Statement

The data that support the findings of this study are available from the corresponding author upon reasonable request.

Keywords

cathode materials, electrochemical properties, $\text{Li}_{0.35}\text{La}_{0.55}\text{TiO}_3$ (LLTO), lithium-ion batteries, X-ray diffraction

Received: July 12, 2022
Revised: September 1, 2022
Published online:

- [1] R. Alcantra, M. Jaraba, P. Lavela, J. L. Tirado, *J. Electroanal. Chem.* **2004**, 566, 187.
- [2] D. Aurbach, B. Markovsky, Y. Talyossef, G. Salitra, H.-J. Kim, S. Choi, *J. Power Sources* **2006**, 162, 780.
- [3] M. G. Lazarraga, L. Pascual, H. Gadjov, D. Kovacheva, K. Petrov, J. M. Amarilla, R. M. Rojas, M. A. Martin-Luengo, J. M. Rojo, *J. Mater. Chem.* **2004**, 14, 1640.
- [4] J. C. Arrebola, A. Caballero, M. Cruz, L. Hernan, J. Morales, E. R. Castellon, *Adv. Funct. Mater.* **2006**, 16, 1904.
- [5] I. Belharouak, W. Lu, D. Vissers, K. Amine, *Electrochem. Commun.* **2006**, 8, 329.
- [6] J. R. Dahn, E. Fuller, M. Obrovac, U. Vonsacken, *Solid State Ionics* **1994**, 69, 265.
- [7] J.-Z. Kong, C. Ren, G.-A. Tai, X. Zhang, A.-D. Li, D. Wu, H. Li, F. Zhou, *J. Power Sources* **2014**, 266, 433.
- [8] J. Shim, S. Lee, S. Park, *Chem. Mater.* **2014**, 26, 2537.
- [9] M. G. Kim, J. Cho, *J. Mater. Chem.* **2008**, 18, 5880.
- [10] J.-H. Wang, Y. Wang, Y.-Z. Guo, Z.-Y. Ren, C.-W. Liu, *J. Mater. Chem. A* **2013**, 1, 4879.
- [11] B. Huang, X. Li, Z. Wang, H. Guo, L. Shen, J. Wang, *J. Power Sources* **2014**, 252, 200.
- [12] Y. Inaguma, C. Liqun, M. Itoh, T. Nakamura, T. Uchida, H. Ikuta, M. Wakihara, *Solid State Commun.* **1993**, 86, 689.
- [13] S.-I. Furusawa, H. Tabuchi, T. Sugiyama, S. Tao, J. T. Irvine, *Solid State Ionics* **2005**, 176, 553.
- [14] O. Maqueda, F. Sauvage, L. Laffont, M. Martínez-Sarrión, L. Mestres, E. Baudrin, *Thin Solid Films* **2008**, 516, 1651.
- [15] Z. Zheng, Y. Wang, *J. Electrochem. Soc.* **2012**, 159, A1278.
- [16] C. L. Liao, C. H. Wen, K. Z. Fung, *J. Alloys Compd.* **2007**, 432, L22.
- [17] Y.-R. Zhu, J. Yuan, M. Zhu, G. Hao, T.-F. Yi, Y. Xie, *J. Alloys Compd.* **2015**, 646, 612.
- [18] H. Zhang, T. Yang, Y. Han, D. Song, X. Shi, L. Zhang, L. Bie, *J. Power Sources* **2017**, 364, 272.
- [19] J. S. Park, X. Meng, J. W. Elam, S. Hao, C. Wolverton, C. Kim, J. Cabana, *Chem. Mater.* **2014**, 26, 3128.
- [20] S. M. George, *Chem. Rev.* **2010**, 110, 111.
- [21] B. Antoniasci, A. H. M. Gonzalez, S. L. Fernandes, C. F. O. Graeff, *Mater. Chem. Phys.* **2011**, 127, 51.
- [22] C. Bohnke, B. Regrag, F. L. Berre, J.-L. Fourquet, N. Randrianantoandro, *Solid State Ionics* **2005**, 176, 73.
- [23] P. Stüble, J. R. Binder, H. Geßwein, *Electrochem. Sci. Adv.* **2021**, <https://doi.org/10.1002/elsa.202100143>.
- [24] I. C. Popovici, E. Chirila, V. Popescu, V. Ciupina, G. Prodan, *J. Mater. Sci.* **2007**, 42, 3373.
- [25] V. Mereacre, N. Bohn, M. Müller, S. Indris, T. Bergfeldt, J. R. Binder, *Mater. Res. Bull.* **2021**, 134, 111095.
- [26] W. Bronger, H. Bade, W. Klemm, *Z. Anorg. Allg. Chem.* **1964**, 333, 188.
- [27] R. Jimenez, A. Rivera, A. Varez, J. Sanz, *Solid State Ionics* **2009**, 180, 1362.
- [28] J. A. Alonso, J. Ibarra, M. A. Paris, J. Sanz, J. Santamaría, C. León, A. Vdrez, M. T. Fernandez, *MRS Proc.* **1999**, 575, 337.
- [29] Y.-J. K. Eun-Tae Kang, *J. Korean Ceram. Soc.* **2003**, 40, 513.
- [30] H. F. Mohamed, *J. Magn. Magn. Mater.* **2017**, 424, 44.
- [31] Y. Kalyana Lakshmi, G. Venkataiah, M. Vithal, P. Venugopal Reddy, *Phys. B* **2008**, 403, 3059.
- [32] R. D. Shannon, *Acta Cryst.* **1976**, A32, 751.
- [33] B. Aktekin, M. Valvo, R. I. Smith, M. H. Sørby, F. Lodi Marzano, W. Zipprich, D. Brandell, K. Edström, W. R. Brant, *ACS Appl. Energy Mater.* **2019**, 2, 3323.
- [34] J. Cabana, M. Casas-Cabanas, F. O. Omenya, N. A. Chernova, D. Zeng, M. S. Whittingham, C. P. Grey, *Chem. Mater.* **2012**, 24, 2952.
- [35] D. Gryffroy, R. E. Vandenberghe, E. Legrand, *Mater. Sci. Forum* **1991**, 79-82, 785.
- [36] A. Feltz, J. Töpfer, B. Neidnicht, *Z. Anorg. Allg. Chem.* **1993**, 619, 39.
- [37] M. Casas-Cabanas, C. Kim, J. Rodríguez-Carvajal, J. Cabana, *J. Mater. Chem. A* **2016**, 4, 8255.
- [38] J. Cabana, H. Zheng, A. K. Shukla, C. Kim, V. S. Battaglia, M. Kunduraci, *J. Electrochem. Soc.* **2011**, 158, A997.
- [39] P. Stüble, S. Indris, M. Müller, H. Gesswein, J. R. Binder, *J. Mater. Chem. A* **2022**, 10, 9010.
- [40] J.-H. Kim, S.-T. Myung, C. S. Yoon, I.-H. Oh, Y.-K. Sun, *J. Electrochem. Soc.* **2004**, 151, A1911.
- [41] M. Schroeder, S. Glatthaar, H. Geßwein, V. Winkler, M. Bruns, T. Scherer, V. S. K. Chakravadhanula, J. R. Binder, *J. Mater. Sci.* **2013**, 48, 3404.
- [42] A. Höweling, A. Stoll, D. O. Schmidt, H. Geßwein, U. Simon, J. R. Binder, *J. Electrochem. Soc.* **2017**, 164, A6349.
- [43] P. B. Samarasingha, N. H. Andersen, M. H. Sørby, S. Kumar, O. Nilsen, H. Fjellvåg, *Solid State Ionics* **2016**, 284, 28.
- [44] J. Tu, X. B. Zhao, D. G. Zhuang, G. S. Cao, T. J. Zhu, J. P. Tu, *Physica B* **2017**, 382, 129.
- [45] T.-F. Yi, Y.-R. Zhu, X.-G. Hu, *Int. J. Miner. Metall. Mater.* **2009**, 16, 119.
- [46] R. Azmi, V. Trouillet, M. Strafela, S. Ulrich, H. Ehrenberg, M. Bruns, *Surf. Interface Anal.* **2018**, 50, 43.
- [47] H. Liu, R. Kloepsch, J. Wang, M. Winter, J. Li, *J. Power Sources* **2015**, 300, 430.

- [48] Z. Zheng, H. Fang, F. Yang, Z.-K. Liu, Y. Wang, *J. Electrochem. Soc.* **2014**, *161*, A473.
- [49] J. C. Arrebola, A. Caballero, L. Hernan, J. Morales, *J. Power Sources* **2010**, *195*, 4278.
- [50] X. Hao, B. M. Bartlett, *J. Electrochem. Soc.* **2013**, *160*, A3162.
- [51] L. Zhou, D. Zhao, X. D. Lou, *Angew. Chem., Int. Ed.* **2012**, *51*, 239.
- [52] J. Xiao, X. Chen, P. V. Sushko, M. L. Sushko, L. Kovarik, J. Feng, Z. Deng, J. Zheng, G. L. Graff, Z. Nie, D. Choi, J. Liu, J. G. Zhang, M. S. Whittingham, *Adv. Mater.* **2012**, *24*, 2109.
- [53] W. Hua, Z. Wu, M. Chen, M. Knapp, X. Guo, S. Indris, J. R. Binder, N. N. Bramnik, B. Zhong, H. Guo, S. Chou, Y.-M. Kang, H. Ehrenberg, *J. Mater. Chem. A* **2017**, *5*, 25391.
- [54] J. H. Scofield, *J. Electron Spectrosc. Relat. Phenom.* **1976**, *8*, 129.